Simultaneous plasmonic measurement of refractive index and temperature based on a D-type fiber sensor with gold wires

Diego Felipe Santos, Ariel Guerreiro, José Manuel Baptista, *Member, IEEE*

***Abstract*— This paper presents an optical fiber sensor that uses surface plasmon resonance (SPR) on metallic wires to directly and simultaneously measure both the refractive index and the temperature. The sensor is constituted by gold wires on a D-type fiber engineered, using numerical simulations based on the finite element method (FEM) to support plasmon modes with strong dependencies to either one of the measured parameters. In particular, the influence of the temperature on the structure of the plasmon modes results from contributions from the thermo-optic effect in the fiber core and sensing layer, and phonon–electron scattering along with electron–electron scattering in the metal wire. The performance of the sensor is evaluated in terms of its sensitivity and resolution.**

***Index Terms*— Finite element method, metallic wires, D-type fiber, optical fiber sensor, refractive index sensor, surface plasmon resonance.**

I. Introduction

In the past years, there has been much research in the development of refractive index sensors based on surface plasmon resonances (SPR) because of their high sensitivity [1]. In particular, SPR sensors use the excitation of a charge-density oscillation (i.e., surface-plasmon wave) along the metal- dielectric interface by p-polarized light, which satisfies certain resonance conditions dependent on the geometric and optical properties of the components and of the analyte medium [2]–[4]. This type of sensor is also used as a biosensor, and consists in one ligand layer, immobilized over the metal, and the analyte flows across it; the changes in the refractive index of the solution allow to characterize the analyte [5]. These sensors can also be adapted to measure other parameters, such as temperature [6] and pressure [7], typically by including components whose size and optical properties strongly depend on each of the desired physical parameter[8]. One of the challenges remaining is the development of simple sensing configurations that can measure simultaneously more than one parameter, such as refractive index and temperature. In fact, the influence of temperature in changing the dimensions and optical properties of the components of the sensor has many times been considered to be an engineering problem that limits the operation of the sensor. For this reason, there is a necessity to have simultaneous measurement of temperature and refractive index.

Sensors based on SPR are notorious for having high sensitivity to variations of refractive index, but the direct impact of temperature changes on the modal structures of surface plasmons results from a combination of a small change in the optical properties and the thermal expansion of the metal. These produces very small wavelength shifts in the plasmon resonances when compared with those produced by changes in the refractive index. One solution is to use separate sensors to do independent measurement of refractive index and of temperature, using distinct sensing principles. Temperature measures are usually based on sensor components that have large thermo-optical or thermal expansion coefficients, usually interferometric in nature and including optical fiber gratings, such as fiber Bragg gratings (FBGs) and long-period fiber gratings (LPGs), as well as, multimode interference and high-birefringence fiber loop mirrors [9], [10].

In SPR sensors, variations of temperature change many of the properties of the fiber (via thermo-optic effect) and of the metal (via phonon–electron scattering along with electron–electron scattering), thus affecting wavelength interrogation, and therefore the sensitivity. In sensors supporting localized SPR, thermal expansion of the different materials may alter dimensions and even further affect the operation of the RI sensor [11].

In this work we address two main challenges. First to measure simultaneously temperature and refractive index of the analyte medium. Second, to have plasmon resonances that present strong dependency to just one of the measures and thus separate their measure. In our proposal, we consider a fiber sensor combining multiple metal wires and supporting several SPR resonances that allows using two wavelengths to measure both temperature and refractive index simultaneously.

This work was supported by the Fundação Para a Ciência e a Tecnologia through the Ph.D. Program under Grant SFRH/BD/85068/2012 and part of project UID/EEA/50014/2013 and also is financed by the ERDF – European Regional Development Fund through the Operational Programme for Competitiveness and Internationalisation - COMPETE 2020 Programme within project «POCI-01-0145-FEDER-006961».

D. F. Santos and J. M. Baptista are with the Centro de Competência de Ciências Exatas e da Engenharia, Universidade da Madeira, Funchal 9000-390, Portugal, and also with INESC TEC Porto, Porto 4169-007, Portugal (e-mail: diegonobregasantos@hotmail.com; jmb@uma.pt).

A. Guerreiro is with the Faculdade de Ciências, Universidade do Porto, Porto 4099-002, Portugal, and also with INESC TEC Porto, Porto 4169-007, Portugal (e-mail: asguerre@fc.up.pt).

II. DESIGN

We consider the design of the refractive index optical sensor composed of a D-type fiber profile with a gold wire mounted on the flat surface, and thus replacing the metallic film usually considered in the literature [12]. Three extra metal wires are implanted in the fiber cladding (as illustrated in Fig. 1. The fiber consists in a conventional step index fiber composed by the core with silica doped with 16% germanium (n_{co}) and surrounded by a pure silica cladding (n_{cl}). The top metal wire is partially embedded on the surface of the fiber cladding to improve mechanical resistance of the device as well as optical coupling to both the core and to the external medium, and this is the external wire with radius r_E. The other three metal wires are placed around the core, embedded in the cladding to increase the sensitivity to temperature and not being exposed to the external medium refractive index, and these are the internal wires with the radius of each wire being r_I. In the computer model, the space surrounding the fiber set is filled with the analytic, referred as the external refractive index n_{ext}. The relevant geometrical parameters are: the distance between the center of the fiber and the center of the external wire and the internal wires defined as d and d_I, respectively and the radius of the fiber core r_{co}.

The metal wire on the surface of the fiber (external wire) is in direct contact with the analyte and therefore supports surface plasmon modes that are primarily sensitive to changes in the external refractive index. On the other hand, the remaining wires (internal wires) support surface plasmon modes that are influenced mainly by changes in the temperature, through their dependency on the optical properties of the metal.

The spectral characteristics of the plasmon modes supported on the external metal wire and the associated resonance are determined mainly by the wire radius (r_E) and the boundary conditions imposed by the refractive index of the external medium. A second plasmon resonance is supported by the remaining internal wires, which depends mainly on their radius (r_I) but also on their relative positions and distances to core of the fiber. These three wires support more than one plasmon mode with distinct sensitivities to the temperature. One of the plasmon modes is selected accordingly, to optimize the sensor performance. In terms of spectral features observed in the imaginary part of the effective refractive index of the fiber sensor, we are able to obtain two resonance peaks, the first peak is used to measure the external refractive index and the second to measure the temperature.

III. THEORY

In this section, we explain the temperature model and the contributions from the thermo-optic effect in the fiber and in the sensing layer. The calculations are done in two steps: first, we calculate the optical properties of the different materials for a given temperature, including the contributions of the phonon–electron scattering and the electron–electron scattering in the case of the metal, and second, we use these values in a computer model based on FEM and implemented in COMSOL to determine the solution of the electromagnetic field equations, corresponding to the optical modes of the sensor. The FEM is becoming the standard method to study the operation of fiber optical sensors with complex geometries [12] and the implementation of this method is explained in detail in reference [13].

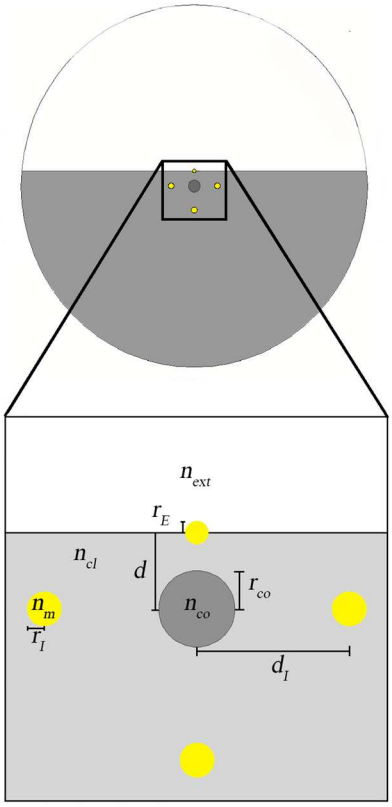

Fig. 1. Schematic of the proposed SPR D-type fiber.

A. Core and cladding

We consider a fiber core of pure silica with a 16% doped GeO_2-SiO_2 glass and the cladding is made out of pure silica. The dependence of the refractive index with wavelength of pure silica and X doped with GeO_2-SiO_2 glass follows the Sellmeier relation according to

$$n=\left\{1+\sum_{i=1}^{3}\frac{\left[B_j^S+X(B_j^G-B_j^S\lambda^2)\right]}{\lambda^2-\left[C_j^S+X(C_j^G-C_j^S)\right]^2}\right\}^{1/2} \quad (1)$$

where B_j^S, C_j^S, B_j^G and C_j^G are the Sellmeier coefficients and the superscripts S and G denote SiO_2 and GeO_2, respectively. The values of these parameters are represented in Table I. The effect of the temperature in the fiber is defined using the

TABLE I SELLMEIER COEFFICIENTS USED TO MODEL THE OPTICAL FIBER [14]

j	B_j^S	C_j^S	B_j^G	C_j^G
1	0.69616630	0.06840430	0.80686642	0.06897260
2	0.40794260	0.11624140	0.71815848	0.15396605
3	0.89747940	9.8961610	0.85416831	11.841931

thermo-optic coefficient (1.28×10^{-5} K) [11], [14].

B. Gold wire

In describing the optical properties of the metal and their dependence on the temperature we adopted the model by Alabastri in [15]. The complex and frequency-dependent dielectric function of any metal can be appropriately represented by the Drude-Lorentz formula in function a frequency (ω)

$$\varepsilon_r(\omega,T)=1-\frac{\Omega_p(T)^2}{\omega\left[\omega-i\Gamma_t(T)\right]}+\sum_{j=1}^{k}\frac{f_j\omega_p^2}{\left(\omega_j^2-\omega^2\right)-i\omega\Gamma_j} \tag{2}$$

where the first term takes into account the contribution from the conduction electrons. The influence of the temperature (T) is included in the parameters $\Gamma_t(T)$ and $\Omega_p(T)$, which correspond to the total collision frequency and the plasma frequency, respectively. The second term describes the interband absorption where k is the number of oscillators with frequency ω_j, strength f_j, and lifetime $1/\Gamma_j$ [16]. The plasma frequency at ambient temperature is defined by

$$\Omega_p=\sqrt{f_0}\omega_p=\sqrt{f_0}\sqrt{\frac{m^*}{4\pi Ne^2}} \tag{3}$$

where N, m^* and e represent the density, the effective mass and the charge of the electrons, respectively, f_0 is the oscillator strength. The plasma frequency varies with temperature due to volumetric effects according to

$$\Omega_p(T)=\Omega_p\left[1+\gamma_e(T-T_0)\right]^{-1/2} \tag{4}$$

where $\gamma_e = 14.2\times10^{-6}$ per K is the expansion coefficient of the metal (Au) and $T_0 = 293.12$ K is the room temperature, which is considered as the reference temperature.

The total collision frequency is given by

$$\Gamma_t(T)=\Gamma_0+\Gamma(T)-\Gamma(T_0) \tag{5}$$

where $\Gamma_0=8.04\times10^{13}$ rad/s is the intraband damping coefficient and $\Gamma(T)$ is the dependence of the collision frequency at the temperature, which depends on two factors: phonon–electron scattering and electron–electron scattering. Their respective contributions are Γ_{cp} and Γ_{ce}.

The phonon–electron scattering can be modeled by using the Holstein model of phonon-electron scattering

$$\Gamma_{cp}(T)=\Gamma_0\left[\frac{2}{5}+4\left(\frac{T}{T_D}\right)^5\int_0^{T_D/T}\frac{z^4dz}{e^z-1}\right] \tag{6}$$

where $T_D = 170$ K is the Debye temperature.

The electron–electron scattering frequency is modeled according to the model proposed by Lawrence, based on the Born approximation and the Thomas–Fermi screening of the Coulomb interaction. The corresponding result can be obtained in terms of the Fermi energy (E_F) of the metal electrons as:

$$\Gamma_{ce}(T)=\frac{1}{6}\pi^4\frac{\Gamma\Delta}{hE_F}\left[(k_BT)^2+\left(\frac{h\omega}{4\pi^2}\right)^2\right] \tag{7}$$

where $\Gamma = 0.55$ is a constant giving the average over the Fermi surface of the scattering probability, $\Delta = 0.77$ is the fractional Umklapp scattering, $E_F = 5.53$ eV is the Fermi energy h is the Planck's constant, k_B is the Boltzmann's constant. Thus (2), together with (4)– (7), completely represent the temperature-dependent dielectric constant of the metal. Apart from its dielectric constant, the thermal expansion of metal film is also important. It should be noted that for the calculation of thermal expansion of the film one should not use the linear thermal- expansion coefficient ($\alpha = 1.42\times10^{-5}$) of the bulk material. Since the wire may only expand into the normal direction, one has to employ a corrected thermal-expansion coefficient α' for the expansion of the film thickness. The corresponding expression is

$$\alpha'=\alpha\frac{(1+\mu)}{(1-\mu)} \tag{8}$$

where $\mu = 0.44$ is the Poisson number of metal. Since μ has a value in the vicinity of 0.3, α' is almost twice the usual thermal-expansion coefficient α, which indicates the importance of this correction [11].

C. Finite element method (FEM)

The study is based on the calculation of the guided modes taking into account both the D-type fiber and the wires, usually referred as supermodes (SMs) since they correspond to the hybridization of the individual modes of each of the structures that compose the device taken isolated, namely the fundamental guided mode of the fiber and the plasmon modes in the wires. All these modes are calculated numerically by solving the wave equation for the Fourier components of the electric field

$$\nabla\times\left[\nabla\times E(r,\omega)-k_0^2\tilde{\varepsilon}_r(r,\omega)\right]E(r,\omega) \tag{9}$$

where ω is the frequency, $E(r,\omega)$ is the electric field, $k_0 = \omega/c$ is the wave-number of the field mode and c is the speed of light. The term $\tilde{\varepsilon}_r$ represents the complex relative dielectric function written in terms of the real part (n_r') and imaginary part (n_r'') of the refractive index, which are then incorporated into the computational model. This term is calculated using (1) for the dielectric components and (2) for the metal (gold) both with the consideration of the temperature. Then, using (9) and the material distribution represented of Fig. 1, we calculate the different plasmonic modes supported by the metal [12], [13].

IV. Study of the Sensor Behavior as Function of the External Refractive Index Variation.

In this section, we study the behavior of the external refractive index sensor in terms of sensitivity and resolution. In this study we have not considered the effect of the temperature, hence the results correspond only to the reference temperature. The sensor parameters used are $d = 2$ µm, $r_{co} = 1$ µm, the radius of the external gold wire is $r_E = 300$ nm. Fig. 2a shows the real part of the effective refractive index of the modes supported by the wires and the fundamental mode of the fiber in the range between 600 to 1000 nm. In this spectral range there are three modes for the external wires (identified with m_E = 0, 1 and 2 depending on the dipole

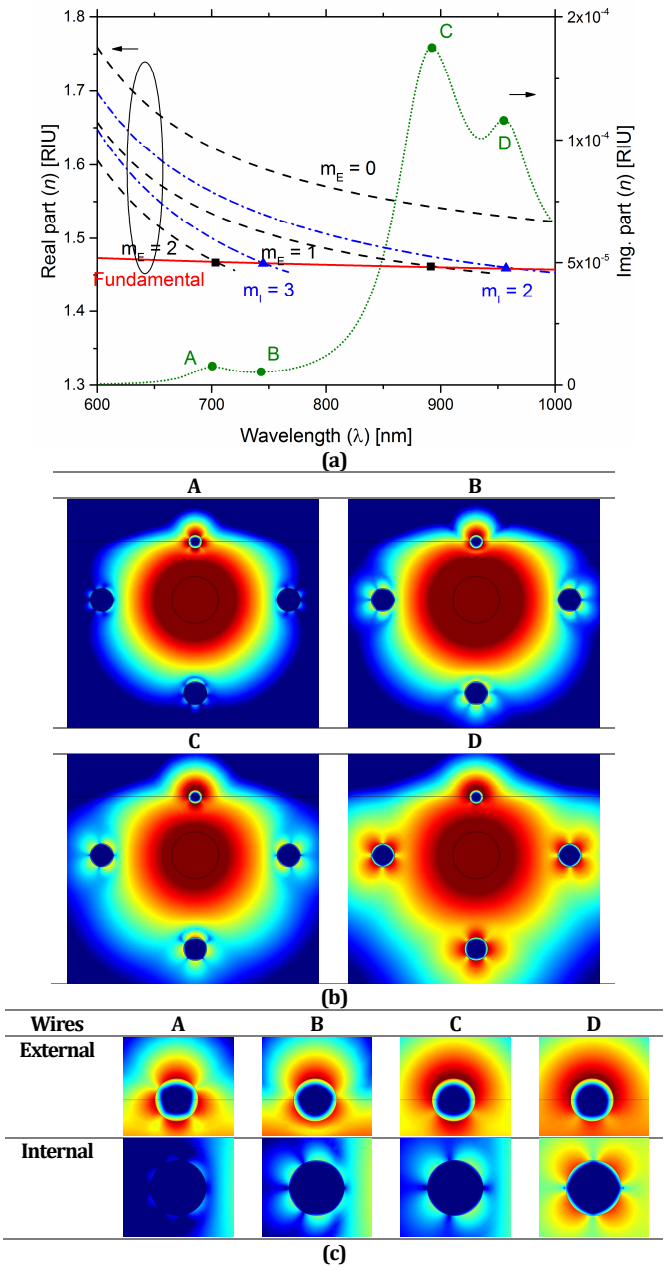

Fig. 2 (a) Real part (solid line) and imaginary part (dot line) of the refractive index of the sensor as function of wavelength for external refractive index of 1.38. Also, we represent the dispersion curves of the metal wires for the external modes, m_E (dashed line) and for the internal modes, m_I (dashed-dot line). The crossing between the dispersion curves of the modes in the metal wires and the fundamental mode of the fiber are indicated by the squared and triangles dots created by the external wire (RI) and the internal wires (*T*), respectively and these points are represented by the circular green circles in the imaginary part of the effective refractive index of the sensor (green dot line). (b) Distribution of the light intensity in the sensor in the referred points. (c) Detail of the distribution of the light intensity near the external and the left internal wire in Fig. 2b.

moment of the modes, respectively with null, dipolar and quadripolar mode), which intercept the fundamental mode of the fiber at two points (black squares in Fig. 2a). Notice that the mode of the external wire with $m_E = 0$ does not couple with the fundamental mode of the fiber, due to poor phase matching conditions, and it is necessary to work with modes with higher *m*. Also, it is necessary to choose the radius of the internal wires (r_I) such that the corresponding resonances do not overlap with those associated with modes supported by the external wire. This produces a spectral separation of the different resonances, which facilitates their independent measurement. In particular, we have chosen $r_I = 500$ nm that supports two modes in the spectral range between 600 to 1000 nm (identified with $m_I = 2$ and 3 and corresponding to modes with quadripolar and hexapolar moments, respectively), as shown in Fig. 2. This solution also intercepts the fundamental mode in two points (blue triangles in Fig. 2a). Fig. 2a also shows imaginary part of the effective refractive index of the sensor (green dotted curve), which shows four resonances (green circles). At points A and C, they correspond to the resonant coupling between the fundamental mode of the fiber and the modes with $m_E = 2$ and $m_E = 1$, and at points B and D they correspond to the resonant coupling between the fundamental mode of the fiber and the modes with $m_I = 3$ and $m_I = 2$. The amplitude of the peaks selected for sensing can be optimized by the distance between the internal wires and the fiber core, therefore controlling the intensity of the coupling between the fundamental mode and each of the internal wire modes. In our case, this optimization resulted in the value $d_I = 4$ µm. The characteristics of the resonance point D are studied in more detail in the next section.

Fig. 2b and 2c show the distribution of the light intensity in the fiber for the resonant wavelengths and illustrates the transition in their characteristics. In all the four cases presented, we clearly identify the contribution from the fundamental mode of the fiber, which determines the distribution of light at the center, while the main differences occur near the wires. At wavelengths near the resonance A, the external wire supports a quadrupole mode ($m_E = 2$), while the modes in the internal wires present six intensity modes in the border of the metal, indicating a predominant hexapolar mode ($m_I = 3$). Near the resonance B, the character of the mode near the external wire transits to a strong dipolar moment. The resonances C and D correspond to an intensity distribution with strong dipolar moment near the external wire and strong quadripolar moment near the internal wires. There is however an important difference in the light distribution of these resonances: while for resonance C the electric field between the internal wires and the core changes sign, for resonance D the sign is preserved. This is similar to the even and odd plasmon modes produced by the coupling of surface plasmons located at opposite surfaces of a thin metal film [17]. he practical difference between these two resonances is that while the resonance C is very sensitive to changes in the refractive index, the resonance D is mainly sensitive to the temperature.

Fig. 3 shows the loss as function of wavelength for different values of the external refractive index of the sensor, with a constant temperature, calculated according to

$$\alpha_{dB} = \frac{20}{\ln(10)}\alpha L \qquad (10)$$

where $\alpha = 2n_{ef}''k_0$ is the power absorption coefficient and *L* is the size of the sensor (1 mm). The sensitivity (*S*) and the

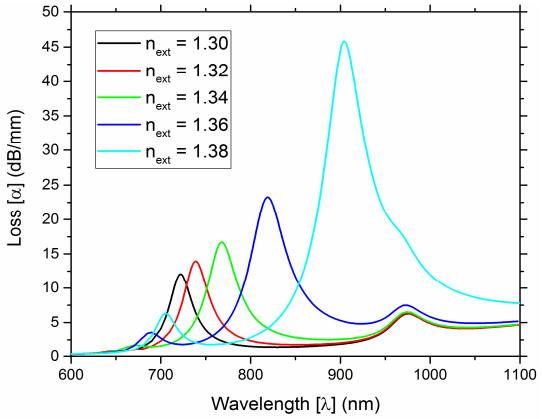

Fig. 3. Loss as function of wavelength for different values of the external refractive index of the sensor with four metallic wires for $d = 2$ µm. The range of the external refractive index is from 1.30 to 1.38. In the curve for n_{ext}=1.38, the two peaks with higher wavelength are partially overlapped, which makes extremely difficult to measure the central wavelength for the weaker peak and therefore limits the range of operation of the sensor.

resolution (R) of the sensor are expressed in Table II and were obtained assuming that it is possible to detect experimentally a spectral variation of 0.1nm and using the data in Fig. 3 and the following equations [6]

$$S(\lambda) = \frac{\Delta\lambda_{peak}}{\Delta n_{ext}} \tag{11}$$

$$R(\lambda) = \frac{1}{S(\lambda)}\Delta\lambda_{\min} = \frac{\Delta n_{ext}\Delta\lambda_{\min}}{\Delta\lambda_{peak}}, \tag{12}$$

where λ_{min} is the minimum value in wavelength between two spectral lines that can be experimentally detected and $\Delta\lambda_{peak}$ is the shift in wavelength of the resonance peak obtained from the simulations for different values of external refractive index (n_{ext}).

The sensitivity and resolution show a good sensor performance when compared with other fiber sensors based on SPR in metal wires. For instance, Luan [18] presented a refractive index sensor where the silver wire is placed on top of the fiber, achieving a sensitivity of 2700 nm/RIU in the wavelength range from 698 to 728nm for n_{ext} = 1.33 to 1.34. Although such sensitivity value is slightly better than in our sensor, it results from the wire being completely exposed, which has the drawback of reducing the robustness of the sensor. Lu [19] presented another refractive index sensor based on grapefruit photonic crystal fiber where the holes are filled with silver wires with radius of 300nm, reaching a sensitivity of 2400nm/RIU for a variation of the external refractive index between 1.33 and 1.335 RI for a wavelength of 635-650 nm, respectively.

TABLE II SENSITIVITY, RESOLUTION AND RANGE OF THE WAVELENGTH VALUES FOR THE REFRACTIVE INDEX OPTICAL FIBER SENSORS

Range of n_{ext}	S(nm/RIU)	Resolution (RIU)	Range λ (nm)
[1.30, 1.32]	687.5	1.45×10^{-5}	720-740
[1.32, 1.34]	1375	7.27×10^{-6}	740-770
[1.34, 1.36]	2437.5	4.10×10^{-6}	770-820
[1.36, 1.38]	4062.5	2.46×10^{-6}	820-900

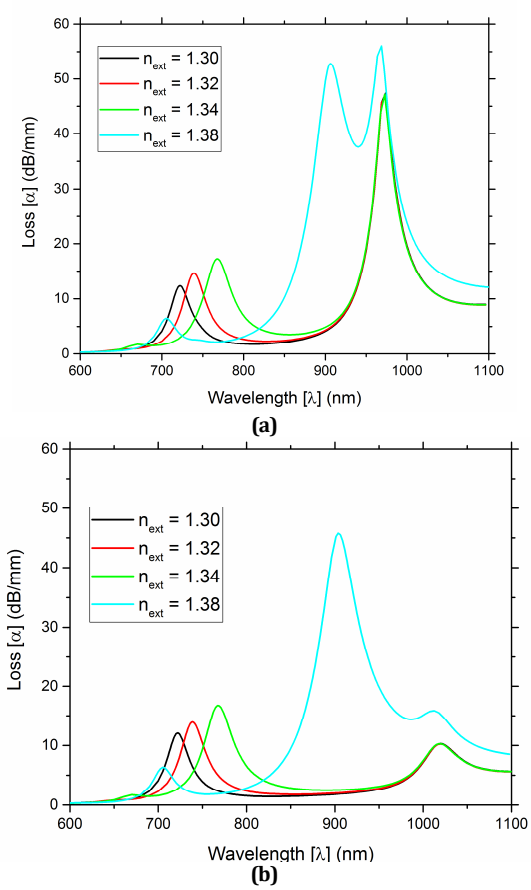

Fig. 4 Loss as function of wavelength for different values of the external refractive index of the sensor D-type for (a) d_1 = 3 µm (the distance between the internal wires and the core) and $r_1 = 500$ nm (radius of the internal wires) and for (b) d_1 = 4 µm and $r_1 = 550$ nm. The external refractive index varies from 1.30 to 1.38.

V. OPTIMIZATION OF THE SENSOR

Fig. 3 shows the loss of the guided mode per unit of length as function of wavelength for different values of the external refractive index, which presents three main peaks. The first, for low wavelengths is very weak and has little use for sensing (λ_{P1}). The second peak is the most intense and shifts towards longer wavelengths with the increasing of the external refractive index (λ_{P2}), whereas the third at higher wavelengths remains unchanged (λ_{P3}). This peak however is much weaker than the second, a problem which can be overcome either by changing the number of internal wires, or by decreasing the distance between the core and internal wires. Another possibility is to lower the intensity of the second peak by changing the distance of the core to the external wire.

The increasing of the number of internal wires can increase this loss peak. However, structures with larger number of wires can be more difficult the fabricate so, we propose a second approach to increase the third peak by reducing the distance between the metal and the internal wires. Fig. 4a

shows the results for the loss if the distance between internal wires and the core is reduced to 1 µm. The reduction of this distance alters the coupling strength between the modes and, in turn, not only shifts the central wavelength of the peaks but also changes their relative amplitudes. However, the dependent character of the second peak (and independent character of the third) on the external refractive index is preserved.

The analysis also shows that the range of measurement of RI of this sensor configuration is between 1.30 and 1.38, and is mainly determined by the geometry and dimensions of the components (specially the metal wires). For higher values of RI, the second and third peaks overlap and it is hard to separate them in the spectrum. This problem can be resolved increasing the radius of the internal wires. Fig. 4b show the loss as function of the wavelength when the radius of the internal wires is 550 nm. This new radius changes only the third peak of resonance from 975 nm to 1025 nm if we compared with the Fig. 3, the first and second peaks maintain the same loss magnitude and wavelength resonance.

Using different parameters like, number of wires, the radius of the internal and external wires and the different distance between the core and the internal and external wires it is possible to optimize the sensor. Our proposal for the sensing configuration considers four wires (one external and three internal) displayed symmetrically around the core as presented in Fig. 1 and with $d = 2.5$ µm, $d_I = 4$ µm, $r_E = 300$ nm (the radius of the external wire) and $r_I = 500$ nm (the radius of the internal wires). With this configuration and parameters, the sensor displays two main peaks with similar amplitude and values of loss that are not excessively high, as well as, and fair peak separation within a range of detection between 1.30 and 1.38, as shown in Fig. 4a.

VI. Study of the Sensor Behavior as Function of the Temperature

In this section we present the behavior of the third peak as function of the temperature. Also, we consider the temperature ambient and the effects of the temperature in the properties of the materials to be modeled according (2).

Fig. 5 shows the loss as function of wavelength for different values of the temperature. The peak on the left corresponds to the second peak (λ_{P2}) observed in the previous figures, while the peak on the right corresponds to the third peak (λ_{P3}). The central wavelength of peak on the left (which is strongly dependent on the external RI) practically does not change with the temperature. Instead, the peak on the right (which is almost independent on the external RI) exhibits a shift toward longer wavelengths for higher temperatures.

The sensitivity of the temperature sensor is calculated according to

$$S(\lambda) = \frac{\Delta\lambda_{peak}}{\Delta T}, \tag{13}$$

where ΔT is the variation in temperature, and, using the data from Fig. 5, we obtain a sensitivity to changes in temperature of 3 pm/K for the peak on the left and the 30 pm/K for the

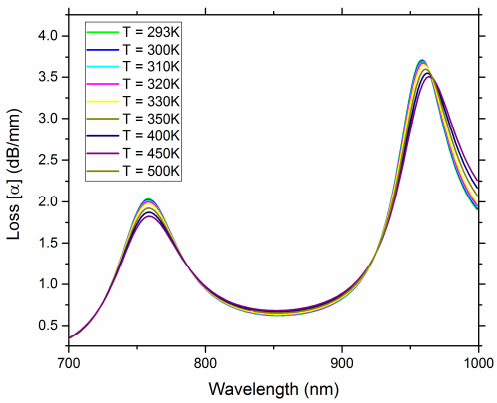

Fig. 5 Loss as function of wavelength for different values of the temperature sensor D-type. The external refractive index is the 1.34 RIU

peak on the right. Although the sensitivity to changes in temperature of the later peak is smaller than other temperature sensors based in SPR found in the literature, it should be noticed that in those cases the measurement of the temperature is assisted by other sensing principles (including thermal expansion of interferometric components), whereas in our case the process is purely plasmonic. Luan [20] used a microstructured optical fiber with a thin layer of silver deposited on the internal surface of one hole, which is then filled with a large thermo-optic coefficient liquid as a sensing medium. This configuration obtained a temperature sensor with high sensitivity of 6.18 nm/K for wavelengths from 838 to 943 nm and with a variation of the temperature from 26 ºC to 43 ºC (which represents a variation of the refractive index of the thermo-optic coefficient liquid from 1.41 to 1.42). Sensors without this type of components have less sensitivity (up to 70 pm/K) [21]. Our configuration is very versatile in the sense that changing geometrical parameters (such as the wire radius or the distance between the wires and the core), the number of wires, among others, it is possible to customize the operation parameters of the sensor, including the range of measurement of the refractive index or the reference wavelength of the sensor. This characteristic surpasses the limitations of other proposals that are dependent on the specific properties of a test fluid[6], [20].

Table III, summarizes the sensitivity coefficients of the two peaks for refractive index (K_n) and temperature (K_T) taken from the information presented in Figs. 3 and 5.

The dual response of the two sensing peaks as function of the variation of the wavelength sensor in terms of RI and temperature, allows writing a conditioned system of two equations for Δn and ΔT, given in matrix form as;

$$\begin{bmatrix} \Delta n \\ \Delta T \end{bmatrix} = \frac{1}{K_{\lambda_{P3},T} K_{\lambda_{P2},n}} \begin{bmatrix} K_{\lambda_{P2},T} & K_{\lambda_{P2},T} \\ 0 & K_{\lambda_{P2},n} \end{bmatrix} \begin{bmatrix} \Delta\lambda_{P3} \\ \Delta\lambda_{P2} \end{bmatrix} \tag{14}$$

where $K_{\lambda_{P2},n}$, $K_{\lambda_{P2},T}$ and $K_{\lambda_{P3},T}$, the matrix elements, are the sensitivity coefficients of the two peaks as function of refractive index and temperature, respectively and represented in Table III.

$$\begin{bmatrix} \Delta n \\ \Delta T \end{bmatrix} = \frac{1}{57.14} \begin{bmatrix} 27.3 & 3.4 \\ 0 & 2093.1 \end{bmatrix} \begin{bmatrix} \Delta\lambda_{P3} \\ \Delta\lambda_{P2} \end{bmatrix} \tag{15}$$

This callibration matrix allows to determine the temperature

Table III SENSITIVITY COEFFICIENTS OF THE TWO PEAKS FOR REFRACTIVE INDEX AND TEMPERATURE.

	K_n	K_T
$\Delta\lambda_{P2}$	2093.1nm/RIU	3.4pm/K
$\Delta\lambda_{P3}$	0	27.3pm/K

and refractive index unequivocally by processing the signals retrieved from the two peaks.

The values of the elements of the calibration matrix presented in Table III show that it is strongly diagonaly dominant and therefore a well conditioned matrix, which will introduce low numerical errors when used to obtain the values of the RI and temperature from the data obtained experimentally. This comes from the dependence of each used peak to a specific sensing parameter (RI and temperature) and thus reducing the crosstalk between them.

These results pave the way for a new type of optical sensors that measure simultaneously different parameters, including temperature and refractive index, via the plasmonic response, which explore both new geometries and other materials that can further improve sensing performances.

VII. CONCLUSION

We have demonstrated a sensor based in a D-type fiber using SPR with multiple wires that allows the simultaneous measurement of temperature and refractive index by direct manipulation of the properties of the surface plasmon resonances supported by the wires. In particular, this sensor presents two main measurement peaks, each resulting from a particular plasmon resonance, and mainly dependent on just one of the two parameters measured, which facilitates the sensor calibration and promotes more accurate measurements. Indeed, in our sensor proposal we verified that one peak is very sensitive to the RI (4000 nm/RIU) and slightly responsive to temperature (3 pm/K), whereas the other peak is only sensitive to the temperature, specifically with a sensitivity of 30 pm/K and practically no response to changes to the refractive index.

We have also shown the possibility to manipulate the supermodes in the wires to obtain a refractive index range detection between 1.30 to 1.38 with a clear distinction of the two measurement peaks, while maintaining the same sensitivity to both parameters (refractive index and temperature). To our knowledge, this has not yet been described in the literature and could, in principle, be extended to even more parameters. This work also aims to stimulate research into the development of novel multiple parameters sensors that use the direct manipulation of the plasmon resonances as sensing principle.

REFERENCES

[1] B. Lee, S. Roh, and J. Park, "Current status of micro- and nano-structured optical fiber sensors," *Opt. Fiber Technol.*, vol. 15, no. 3, pp. 209–221, Jun. 2009.

[2] Z. Tan, X. Hao, Y. Shao, Y. Chen, X. Li, and P. Fan, "Phase modulation and structural effects in a D-shaped all-solid photonic crystal fiber surface plasmon resonance sensor," *Opt. Express*, vol. 22, no. 12, p. 15049, 2014.

[3] G. An, S. Li, W. Qin, W. Zhang, Z. Fan, and Y. Bao, "High-Sensitivity Refractive Index Sensor Based on D-Shaped Photonic Crystal Fiber with Rectangular Lattice and Nanoscale Gold Film High-Sensitivity Refractive Index Sensor Based on D-Shaped Photonic Crystal Fiber with Rectangular Lattice and Nanoscale Gol," *Plasmonics*, vol. 9, pp. 1355–1360, 2014.

[4] J. Homola, H. B. Lu, G. G. Nenninger, J. Dostálek, and S. S. Yee, "A novel multichannel surface plasmon resonance biosensor," *Sensors and Actuators, B: Chemical*, vol. 76, no. 1–3. pp. 403–410, Jun-2001.

[5] R. Verma and B. D. Gupta, "A novel approach for simultaneous sensing of urea and glucose by SPR based optical fiber multianalyte sensor.," *Analyst*, vol. 139, no. 6, pp. 1449–55, 2014.

[6] N. Luan, R. Wang, W. Lv, Y. Lu, and J. Yao, "Surface plasmon resonance temperature sensor based on photonic crystal fibers randomly filled with silver nanowires.," *Sensors (Basel).*, vol. 14, no. 9, pp. 16035–45, Jan. 2014.

[7] A. Belahmar and A. Chouiyakh, "Investigation of Surface Plasmon Resonance and Optical Band Gap Energy in Gold / Silica Composite Films Prepared by RF-Sputtering," vol. 2, no. 2, pp. 81–84, 2016.

[8] Y. Zhao, Z.-Q. Deng, and H.-F. Hu, "Fiber-Optic SPR Sensor for Temperature Measurement," *IEEE Trans. Instrum. Meas.*, vol. 64, no. 11, pp. 3099–3104, 2015.

[9] H. Tao, Y. Zhao, A. Song, T. Hu, Y. Zhao, and A. Song, "Fiber optic SPR sensor for refractive index and temperature measurement based on MMF-FBG-MMF structure," *Sensors Actuators B Chem.*, vol. 237, pp. 521–525, 2016.

[10] C. Gouveia, G. Chesini, C. M. B. Cordeiro, J. M. Baptista, and P. A. S. Jorge, "Simultaneous measurement of refractive index and temperature using multimode interference inside a high birefringence fiber loop mirror," *Sensors Actuators, B Chem.*, vol. 177, pp. 1717–1723, Feb. 2013.

[11] A. K. Sharma and B. D. Gupta, "Influence of temperature on the sensitivity and signal-to-noise ratio of a fiber-optic surface-plasmon resonance sensor.," *Appl. Opt.*, vol. 45, no. 1, pp. 151–161, 2006.

[12] D. F. Santos, A. Guerreiro, and J. M. Baptista, "Numerical investigation of a refractive index SPR D-type optical fiber sensor using COMSOL multiphysics," *Photonic Sensors*, vol. 3, no. July, pp. 61–66, Aug. 2012.

[13] I. Moldovean and I. G. Tarnovan, "Analysis Of Linearly Polarized Modes," in *COMSOL Conference 2012 Boston*, 2012.

[14] J. W. Fleming, "Dispersion in GeO 2 -SiO 2 glasses," *Appl. Opt.*, vol. 23, no. 24, pp. 4486–4493, 1984.

[15] A. Alabastri, S. Tuccio, A. Giugni, A. Toma, C. Liberale, G. Das, F. De Angelis, E. Di Fabrizio, and R. P. Zaccaria, "Molding of plasmonic resonances in metallic nanostructures: Dependence of the non-linear electric permittivity on system size and temperature," *Materials (Basel).*, vol. 6, no. 11, pp. 4879–4910, 2013.

[16] A. D. Rakic, A. B. Djurisic, J. M. Elazar, and M. L. Majewski, "Optical properties of metallic films for vertical-cavity optoelectronic devices.," *Appl. Opt.*, vol. 37, no. 22, pp. 5271–5283, 1998.

[17] M. Yamamoto, "Surface Plasmon Resonance (SPR) Theory : Tutorial," *October*, vol. 48, no. July, pp. 1–32, 2008.

[18] N. Luan and J. Yao, "Surface Plasmon Resonance Sensor Based On Exposed-Core Microstructured Optical Fiber Placed With A Silver Wire," *IEEE Photonics J.*, vol. 8, no. 1, pp. 1–8, 2016.

[19] Y. Lu, C.-J. Hao, B.-Q. Wu, X.-H. Huang, W.-Q. Wen, X.-Y. Fu, and J.-Q. Yao, "Grapefruit fiber filled with silver nanowires surface plasmon resonance sensor in aqueous environments.," *Sensors (Basel).*, vol. 12, no. 9, pp. 12016–25, Jan. 2012.

[20] N. Luan, C. Ding, and J. Yao, "A Refractive Index and Temperature Sensor Based on Surface Plasmon Resonance in an Exposed-Core Microstructured Optical Fiber," *IEEE Photonics J.*, vol. 8, no. 2, pp. 1–8, 2016.

[21] T. Srivastava, R. Das, and R. Jha, "Highly Sensitive Plasmonic Temperature Sensor Based on Photonic Crystal Surface Plasmon Waveguide," *Plasmonics*, vol. 8, no. 2, pp. 515–521, 2012.

Diego Felipe Santos was born in Venezuela in 1987. He received the degree in Electronics and Telecommunications Engineering in 2010 and the Master degree Telecommunications and Energy Networks Engineering in 2012, both from the University of Madeira, Portugal. He is currently doing a Ph.D. in to Automation and Instrumentation with the University of Madeira in collaboration with the INESC TEC Porto, Portugal. His research interests include the design and simulation of optical fiber sensors.

Ariel Guerreiro graduated in "Physical Engineering" from the Technical University of Lisbon, Lisbon, Portugal, in 1998, and obtained his PhD in "Physical Engineering" at the same University in 2004. Currently, he is an Assistant Professor and the director of the graduation course in Physics at the University of Porto, Portugal. He is also Senior Researcher in the Optoelectronics and Electronics Systems Unit at INESC TEC Porto, Portugal. His main scientific areas are quantum and nonlinear optic, nanoplasmonics and their application in optical sensing. He is author of more than 50 journal publications, 40 communications in national and international conferences, 1 book chapter, recipient of one national and one international scientific prizes, reviewer of several scientific publications and member of various international scientific organizations.

José Manuel Baptista (M'03) graduated in "Electrical and Computer Engineering" from the University of Porto, Porto, Portugal, in 1991, followed by the M.Sc. degree in "Physics of Laser Communications" from the University of Essex, Colchester, U.K., in 1993, and then he obtained the Ph.D. degree in "Electrical and Computer Engineering" from the University of Porto, in 2002. Currently, he is the Vice-Rector of the University of Madeira for Research and International Relations. He is Associate Professor at the Faculty of Exact Sciences and Engineering in the University of Madeira, Portugal. He is also Senior Researcher in the Optoelectronics and Electronics Systems Unit at INESC TEC Porto, Portugal. His main scientific areas are the fiber optic sensors, fiber optic communications and fiber optic technologies. He is author of 77 journal publications, 112 communications in national and international conferences, 3 chapter books, 2 patents, and reviewer of several scientific publications and member of various international scientific organizations.